**Structure-based Discovery of Novel non-Covalent Small Molecule Inhibitors of USP30**

Padmanabhan Anbazhagan, Jothi Anantharajan, Justina Fulwood, Marcus Low, Nithya Baburajendran, Klement Foo, Weijun Xu*

Experimental Drug Development Centre, 10 Biopolis Rd, Chromos, Agencey for Science, Technology and Research (A*STAR), Singapore, 138670

*Corresponding author: WX: Xu_weijun@eddc.sg

ORCID: 0000-0002-3566-1082

**Abstract**

Ubiquitin-specific proteases (USPs) are crucial regulators of protein degradation pathways, influencing diverse cellular processes and disease mechanisms. Among them, USP30 plays a pivotal role in mitochondrial quality control and has been implicated in idiopathic pulmonary fibrosis (IPF), a chronic lung disease for which current therapies merely slow disease progression. The high flexibility of USP30's catalytic site, coupled with its dependence on covalent interaction with the catalytic cysteine presents significant challenges in discovering suitable small molecule inhibitors. In this study, we successfully identified three non-covalent small molecule inhibitors for USP30 using molecular modeling, x-ray crystallography, and virtual screening. These findings offer valuable insights and novel chemical starting points for further medicinal chemistry optimization.

**Keywords:** USP30, Ubiquitin, virtual screening, non-covalent inhibitor, deubiquitinating enzymes (DUBs), Ubiquitin-Specific Proteases (USPs), idiopathic pulmonary fibrosis (IPF), Mission Therapeutics compound, Vincere Biosciences (VB)

## Introduction

Deubiquitinating enzymes (DUBs) form a diverse group of approximately 100 proteases, categorized into six major families based on their sequence, domain homology[1], and catalytic mechanisms[2,3]. Among these, ubiquitin-specific proteases (USPs) represent the largest family, comprising over 50 members. USPs play essential roles in regulating protein stability, cellular signaling, and various biological processes[4]. They share a conserved catalytic domain known as the ubiquitin-specific protease (USP) domain, which features a characteristic architecture of palm, thumb, and finger subdomains[4,5], housing the residues critical for enzymatic activity. Dysregulation of USPs has been implicated in a range of diseases, including cancer, neurodegenerative disorders, and inflammatory conditions[1]. USPs therefore represent compelling targets for drug development, offering significant opportunities for advancing therapeutic strategies[1]. Among the approximately 50 USPs, ubiquitin-specific protease 30 (USP30) is considered as a key regulator of mitochondrial dynamics and homeostasis[6]. Uniquely localized to the outer mitochondrial membrane, USP30 modulates the ubiquitination status of proteins essential for mitochondrial quality control, including mitophagy[6,7,8]. This regulatory role is critical for preventing the accumulation of damaged mitochondria, a hallmark of age-related diseases such as Parkinson's disease, Alzheimer's disease, and certain cancers[8,9,10]. In recent years, USP30 has attracted increasing attention as a drug target for pulmonary disorders, including chronic obstructive pulmonary disease (COPD) and idiopathic pulmonary fibrosis (IPF). IPF is a severe lung disease characterized by progressive fibrosis and declining lung function[11,12]. USP30 plays a pivotal role in mitophagy, the selective degradation of damaged mitochondria is crucial for maintaining mitochondrial integrity in pulmonary cells[11,12]. Targeting USP30 inhibition has the potential to mitigate mitochondrial dysfunction, a key contributor to IPF pathogenesis. The inhibition of USP30 activity has been shown to enhance mitophagy, thereby improving mitochondrial quality and function in disease models[13,14]. However, the intricate signaling pathways regulating USP30 activity and its broader implications for cellular physiology remain poorly understood. Additionally, the development of specific USP30 inhibitors poses significant challenges due to the enzyme's structural similarity to other members of the USP family, necessitating a deeper understanding of its structure-function relationships[15].

Vincere Biosciences (VB) patented a series of USP30 inhibitors aimed at enhancing mitophagy and improving mitochondrial function (International Publication Number WO2022192562A1)[16]. These inhibitors demonstrated potent inhibition of USP30 activity in

vitro and showed preclinical efficacy in neuroprotection, particularly for Parkinson's disease[17,18]. Mission Therapeutics developed USP30 covalent inhibitors targeting a range of diseases, including renal conditions such as chronic kidney disease (CKD), idiopathic pulmonary fibrosis (IPF), neurodegenerative diseases, and rare mitochondrial disorders[19]. Notably, MTX-652 and MTX-325 (developed by Mission Therapeutics) are currently undergoing clinical evaluation for kidney diseases (Phase 2) and Parkinson's disease (Phase 1), respectively[20]. Although compounds developed by these companies are in clinical setting, the relatively large molecular weight and peptidomimetic nature of the inhibitors from Vincere Biosciences, as well as potential loss of specificity at higher concentrations observed in covalent inhibitors like cyanopyrrolidines[21,22,23] warrant the need for the development of novel USP30 inhibitors with enhanced selectivity, improved pharmacokinetics, and a favorable safety profile to address unmet clinical needs.

Here, we employed a combination of computational approaches and x-ray crystallography to identify novel non-covalent USP30 inhibitors. After two rounds of virtual screening from Enamine drug-like library and testing of 260 synthesized compounds, we validated three hits (Compound **3** $IC_{50}$ 41.2 μM, Compound **4** 55.7 μM and Compound **5** 57.1 μM) in a biochemical assay. Despite moderate potency, our findings provide valuable structural scaffolds that can serve as templates for future medicinal chemistry efforts, advancing the development of new therapeutics targeting USP30.

**Methods:**

*Protein structure preparation:*

The crystal structure of human USP30 (PDB ID: 5OHP) was obtained from the Protein Data Bank (https://www.rcsb.org/)[24]. The structure was prepared using the Protein Preparation Wizard in Maestro (Schrödinger Suite 2022-3, Version 13.3.121)[25]. Protonation states of protein residues were assigned at a physiological pH of 7.4, and missing hydrogen atoms were added. Bond orders were corrected, and hydrogen bonds were optimized to resolve structural uncertainties. The structure was then subjected to restrained minimization using the OPLS4 force field, enabling full optimization of hydrogen atoms while restricting heavy atom movements to a maximum root mean square deviation (RMSD) of 0.30 Å.

*Preparation of ligands:*

Compounds I-1, I-20 and I-23 from Vincere Biosciences Inc. (WO 2021/050992 A1) was obtained from a published patent[16]. The 2D molecular structure was constructed using ChemDraw and imported into the Maestro molecular interface (version 13.3.121) of the Schrödinger Suite[25]. Ligand preparation was performed using the LigPrep module to generate 3D structures suitable for molecular docking (Schrödinger)[25]. Potential ionization states were calculated at a physiological pH of 7.4. All other parameters were kept at default settings, and energy minimization of the ligands was carried out using the optimized potential for liquid simulations (OPLS4) force field.

*Sitemap and Induced-fit Docking:*

The druggability of USP30 was assessed using the SiteMap tool[26] in Schrödinger (default settings), which identified potential binding sites. The highest-ranked binding region predicted by SiteMap was selected, and its residues were defined as the centroid for induced-fit docking (IFD). The IFD process involved the Vincere Biosciences Inc.'s patented compound (Compound I-1, herein referred to as compound **1** in this study) and was conducted using the Induced Fit Docking module in Maestro v9.1[25]. The protocol generated 20 poses for the compound **1**. Residues within 5.0 Å of the ligand poses were refined during the prime side-chain optimization step to ensure proper ligand-receptor fit. Following this, Glide SP redocking was performed on receptor-ligand structures within 30.0 kcal/mol of the optimal docking score, selecting the top 20 ranked poses overall.

*Covalent docking:*

The pre-processed USP30 crystal structure (PDB ID: 5OHP) was used for covalent docking using the CovDock workflow within the Schrödinger software suite. Covalent docking was performed to explore the binding mode of the Mission Therapeutics compound (herein referred to as compound **2**). The reaction type was specified as "nucleophilic addition to a triple bond," and the docking mode was set to "thorough pose prediction" to ensure accurate modeling of ligand-receptor interactions. Since the 5OHP structure contains the Cys77Ala mutation, an *insilico* mutation was introduced to revert Ala77 back to the native cysteine (Cys77) prior to conducting the covalent docking experiments. This step ensured that the catalytic cysteine, a key residue for covalent binding, was appropriately modeled for the docking studies.

*Ultra-large Scale Virtual Screening:*

The Enamine drug-like library, consisting of 32 million compounds representing the REAL drug-like space, was utilized for virtual screening. The library includes diverse compounds adhering to drug-likeness criteria such as Lipinski's "Rule of 5" and Veber's guidelines (MW ≤ 500, SlogP ≤ 5, HBA ≤ 10, HBD ≤ 5, rotatable bonds ≤ 10, and TPSA ≤ 140), while excluding PAINS and toxic compounds. The screening process combined active learning with Glide docking (Schrödinger) under default settings. Ligands were prepared at pH 7.4, generating up to 16 stereoisomers per compound. The workflow involved three iterations of molecular docking and machine learning. Initially, 50,000 diverse compounds were randomly selected for Glide SP docking, and the results were used to train a machine learning model in the Active Learning module. Based on docking scores, the model evaluated the entire library to select the next 50,000 compounds, and a total of 100,000 compounds underwent Glide SP docking and further model refinement in the second iteration. A similar process was repeated in the third iteration, after which the model predicted docking scores for the entire library, and the top 1 million compounds were re-scored using the Glide SP scoring function. All computations were performed on the EDDC-GLIDE server using 225 CPUs, ensuring efficient processing of the large dataset.

*USP30 catalytic domain cloning, protein expression and purification*

The human USP30 catalytic domain construct (aa 64–502, mutations: F348D, M350S, I353E; Box 4/5 deletion D (358–431) SNA; Box 2/3 deletion D (179–216) GSGS) was designed for structural studies as previously described[24]. A codon-optimized gene encoding an N-terminal His6 tag, a PreScission protease cleavage site, a glutathione S-transferase (GST) tag, and another PreScission protease cleavage site, followed by the USP30 catalytic domain sequence, was synthesized and cloned into the pGEX-6P-1 vector. The recombinant protein was expressed in *E. coli* strain Rosetta2 (DE3), with cells grown at 30 °C until the OD600 reached 0.8. Protein expression was induced using 1 mM isopropyl-β-D-thiogalactopyranoside (IPTG) at 18 °C for 18 hours. Harvested cells were resuspended in lysis buffer (50 mM sodium phosphate pH 8, 300 mM NaCl, 5 mM β-mercaptoethanol, 20 mM imidazole, and a protease inhibitor cocktail) and lysed using a probe sonicator. The clarified supernatant was subjected to purification on a gravity column containing nickel NTA agarose resin. The purified protein underwent tag cleavage using PreScission protease, followed by reverse $Ni^{2+}$ affinity chromatography to purify the tag-cleaved protein sample. The sample was dialyzed against buffer (25 mM Tris pH 8, 50 mM NaCl, 5 mM DTT) to achieve a homogeneous preparation with >95% purity. Further purification was performed using anion exchange chromatography.

For crystallization, the protein sample was prepared by mixing 18 μM of USP30 catalytic domain with 250 μM of inhibitor, followed by incubation at 4 °C for 20 hours. The mixture was then subjected to gel filtration chromatography on a HiPrep 16/60 Superdex S-75 column. The protein sample was concentrated to 12 mg/mL and stored in 20 mM Tris pH 8, 100 mM NaCl, and 5 mM DTT.

*Crystallization setup*

Co-crystals of USP30 with compound **2** were obtained using the hanging drop vapor diffusion method. Drops containing a 1:1 (v/v) ratio of protein to reservoir solution (200 mM ammonium citrate tribasic pH 7, 20% w/v polyethylene glycol 3,350) were incubated at 20 °C. The crystals were cryoprotected using 25% v/v glycerol and flash-frozen in liquid nitrogen prior to data collection. X-ray diffraction datasets were collected at the MX2 beamline at the Australian Synchrotron[27]. Data processing and scaling were performed using the XDS program[28]. The crystal structure was solved via molecular replacement using PHASER MR in PHENIX[29], with a USP30 structure (PDB ID: 5OHK) as the starting model. Subsequent model building and iterative refinement were carried out using COOT[30] and PHENIX[31].

A second round of virtual screening was conducted using our in-house solved X-ray structure of USP30, following the same protocol as described under *Ultra-large Scale Virtual Screening*. However, after the active learning/Glide virtual screening stage, the top 20,000 compounds were selected for further analysis. To refine the results, the DISE selection method was applied, yielding 300 diverse hit clusters for subsequent investigation.

***USP inhibition assay***

Compounds were serially diluted 3-fold, 10 points starting with 10 mM in 100% DMSO. Compounds were then dispensed into 384 well-black low-volume plates (Corning 3821) using the ECHO 650 (Labcyte) liquid handler. Compounds were dispensed in duplicate wells. An amount of 100 nl of compound was dispensed to a total reaction volume of 10 μl, producing a highest concentration of compound of 100 μM. His-tagged recombinant human USP30 protein ((rhUSP30; amino acids 57–517 of the full-length protein, and a C-terminal 6-His tag, Sf 21 (baculovirus)-derived human USP30 protein) (5 nM; final assay concentration = 2.5 nM; RnD Systems) was prepared in USP30 activity assay buffer (50 mM Tris base pH 8.0, 50 mM NaCl,

0.05% BSA, 0.002% Tween 20, 1 mM DTT) and 5µl of dissolved protein was dispensed into a pre-dispensed assay plate containing compounds using a Multidrop bulk dispenser (Thermo Scientific). The protein and compound mixture was then incubated for 30 min at room temperature in the dark. Following incubation, 5 µl of concentrated ubiquitin-rhodamine 110 (Ub-Rho110) (50 nM, final assay concentration = 25 nM; RnD Systems), prepared in USP30 activity assay buffer, was dispensed into the compound-rhUSP30 containing plate and incubated for another 90 min at room temperature in the dark. Fluorescence was then measured using Tecan M1000 plate reader, at excitation wavelength of 485 nm and emission wavelength of 535 nm.

***Chemistry***

## Results

### *Structural assessment of USP30*

To understand the molecular architecture of USP30's binding site, a detailed structural assessment was conducted. The three-dimensional structure of USP30 features the finger, thumb, and palm domains (Figure 1A). Examination of the di-ubiquitin-bound USP30 structure revealed that the substrate sequence, encompassing Arg72 (P5), Leu73 (P4), and Arg74 (P3), adopts a "T"-shaped conformation, with Leu73 deeply buried within the catalytic site (Figure 1B). This analysis was further supported by a comparative study of USP30 structures and co-crystal structures of other ubiquitin-specific proteases (USPs) complexed with potent inhibitors, including USP7 in complex with 8RN a potent inhibitor (PDB ID: 5N9R)[32] and USP14 in complex with IU1 (PDB ID: 6IIK)[33]. These structural comparisons provided critical insights into the configuration of the USP30 catalytic binding site and the interactions that potential inhibitors might exploit. Together, these findings lay the foundation for understanding the structural requirements for small molecule binding and guide the design of novel inhibitors. The comparative structural analysis highlights that, despite some variability in the surface loops and flexible regions of USPs, a conserved core ubiquitin-binding domain is present across these enzymes[34,35]. This conservation suggests that the binding site observed in other USPs may also be exploited in USP30. Notably, the catalytic triad and adjacent residues, which form the active site in other USPs, are structurally conserved in USP30, reinforcing its potential as a viable target for small-molecule inhibitors. Analysis of the co-crystal structures of USP7 and USP14 revealed that the phenyl ring of the inhibitor occupied a deep hydrophobic pocket within the

catalytic site (supplementary figures 1 and 2), possibly mimicking the P4 Leu73 from the natural substrate.

***Docking of literature compounds into the USP30 crystal structure***

Various inhibitors have been reported for different USP family members (Figure 2A). For USP30, despite the small size of its binding site, the Dscore calculated by SiteMap (0.99) indicated the presence of a potential druggable pocket for small-molecule ligands (Figure 1C). Residues identified by SiteMap were used as centroids for receptor grid generation (See method for detail). Unfortunately, initial attempts to dock compound **1** using Glide SP docking were unsuccessful, as the sidechains of Lys338 and His340 obstructed the aromatic ring of compound **1** from positioning deeply within the pocket. To overcome this, the sidechains of Lys338 and His340 were manually adjusted to allow better accommodation of the compound. Subsequently, induced-fit docking was employed, successfully positioning compound **1** within the catalytic pocket (Figure 2B). The docked pose of compound **1** revealed that the phenyl ring and indole moiety of the compound formed π-stacking interactions with His444, while the sulfonamide NH moiety established a hydrogen bond with Glu164 (Figure 2B). To gain confidence in our modeling, we docked additional Vincere Biosciences compounds (e.g. I-20 and I-23) to the pocket hypothesized for accommodating compound **1.** In congruent with our prediction, the overlaid structures (supplementary figure 3) demonstrate that multiple VB compounds can bind into the proposed pocket, with the common phenyl ring moiety wedged within the central deep hydrophobic pocket In addition, our results align with a recently published study, which demonstrated that the fluorophenyl ring of congeneric ligands fit into the deep pocket, forming π-stacking interactions with His444[36]. Additionally, the repositioning of sidechains near the catalytic site increased the hydrophobicity of the pocket, resulting in a Dscore of 1.03.

Next, we sought to model the molecular interaction between a covalent inhibitor (mission therapeutics compound **2**) and USP30. The USP30-compound **1** docked complex provides a reasonable starting conformation for covalent docking of compound **2**. For compound **2**, a covalent adduct with Cys77 was anticipated, formed via the reaction illustrated below:

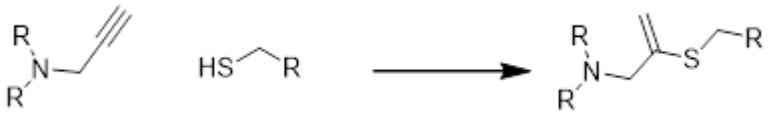


Customized covalent bond formation from Schrödinger

We then customized a covalent reaction using the following syntax:

RECEPTOR_SMARTS_PATTERN 2,[C,c]-[S,O;H1,-1]

LIGAND_SMARTS_PATTERN 1,C#C[H]

CUSTOM_CHEMISTRY ("<1>",("charge",0,1))

CUSTOM_CHEMISTRY ("<1>|<2>",("bond",1,(1,2)))

CUSTOM_CHEMISTRY ("<2>#C",("bond",2,(1,2)))

The predicted binding mode and pocket occupied by compound **2**, as determined through our modeling efforts, is shown in Figure 3A. Compound **2** is positioned between the thumb and palm domains, a region that guides the ubiquitin C-terminus into the catalytic site. We further validated our docking results by comparing them with the recently published structure of the USP30 catalytic domain in complex with a covalent inhibitor (PDB ID: 8D0A, Figure 3B), which revealed a good overlay between compound **2** and the covalent inhibitor, as shown in Figure 3C. Our docking predictions align well with findings from a recent study[37], further supporting the reliability of our modeling efforts.

**Virtual screening identifies three inhibitors of USP30**

Next, we conducted a virtual screening campaign using the compound **1** trained USP30 structure against the Enamine drug-like database, comprising ~32 million compounds. The complete workflow is outlined in Figure 4A. The whole screening campaign spanned 20 days on a 256 CPU-cluster, demonstrating efficiency for ultra-large-scale screening. Specifically, virtual screening was executed on a 128-CPU cluster with 50 parallel jobs for Glide SP docking, while DeepChem-based machine learning utilized an NVIDIA V100 Tensor core GPU. Following the active learning/Glide workflow, the top 1 million ligands predicted by the active learning model were rescored by Glide SP docking. Post-screening, the top 10,000 compounds ranked by Glide SP scores were selected for further analysis, and unique compounds were retained for prioritization. Analysis of the virtual screening results revealed three predominant binding conformations: an inverted "L" shape, a "7" shape, and a "T" shape

(Supplementary Figure 4). Two approaches were applied to prioritize virtual hits: (1) Diversity-based selection from the top 17,000 compounds, which identified 10,000 diverse candidates grouped into 600 clusters based on fingerprint similarity; and (2) Volume-overlap ligand clustering, which grouped the top 8,000 compounds into 141 clusters based on volume alignment. Each cluster was visually inspected, focusing on compounds adopting the "7" and "T" shape conformations. Filtering criteria, visual inspection, Strain Penalty > 2, total charge > 2, rotatable bonds > 7, and overall shape of the pocket and ligand fitness, were applied, resulting in a final selection of 125 promising compounds. Of these, 90 successfully synthesized compounds were tested in-house. One compound, Compound **3**, exhibited an IC50 of 41.2 μM (Figure 4B). Redocking of **3** suggested that it adopts a "7"-shaped conformation, with its phenyl ring positioned deep within the pocket, forming a π-π stacking interaction with the highly conserved His444 residue (Figure 4C). In-house sequence alignment studies (unpublished data) further confirmed the conservation of His444 within the USP family, suggesting that this residue may play a critical role in stabilizing the phenyl ring within the catalytic pocket.

During the *In Silico* covalent docking studies using the model trained by compound **1**, our in-house X-ray crystallography resolved the structure of the USP30 catalytic domain bound to compound **2** at a resolution of 2.58 Å (Figure 5A). The overall structure of the USP30 catalytic domain (CD) in complex with compound **2** adopts a fold similar to previously determined USP30~Ub-PA (PDB ID: 5OHK) and USP30–Lys6-diubiquitin complexes (PDB ID: 5OHP). Consistent with our docking model, compound **2** binds at the thumb-palm cleft and forms a covalent adduct with the catalytic Cys77 of USP30 (Figure 5A). The compound **2** binding pocket is primarily stabilized by hydrophobic interactions involving residues Met448, Phe453, and the aromatic ring of Tyr495, as well as multiple hydrogen bonds with Gly74, Gly451, Asp447, Met448, His444, and Asn72 of USP30 (Figures 5B and 5C). Superposition of the USP30-compound **2** complex and the USP30–Lys6-diubiquitin complex (PDB ID: 5OHP) revealed significant structural rearrangements in the finger subdomain and loops surrounding the catalytic site. These include changes in the preceding loop to the catalytic Cys77 (residues 70–78), blocking loop 1 (residues 322–340), and blocking loop 2 (residues 446–456), as well as a lack of electron density for the switching loop region (residues 151–160) (Figure 5D). In the USP30–compound **2** complex, the side chain of Met448 in blocking loop 2 undergoes significant repositioning compared to the USP30-diubiquitin complex. This repositioning

enables Met448 to form both a hydrophobic interaction and a hydrogen bond with compound **2** (Figure 5D). Additionally, Asn72 in the preceding loop to Cys77 forms a hydrogen bond with compound **2**, whereas in the USP30–diubiquitin complex, Asn72 forms a hydrogen bond with Thr12 in the β2 strand of proximal ubiquitin (Figure 5D). Superimposition of the compound **2** docked pose to the in-house co-crystal structure revealed a reasonable overlay, with a root-mean-square deviation (RMSD) of 1.6 Å (Figure 5E), validating the accuracy of our docking predictions. The data collection and refinement statistics for the USP30-compound **2** co-crystal structure are summarized in Table 1. We next performed a second round of virtual screening based on the in-house solved X-ray structure of USP30 using the same virtual library mentioned above. The complete workflow is illustrated in Figure 6A. Structure and ligand preparation followed the protocols outlined in the Methods section. The selection criteria for compounds were based on multiple factors, including docking scores, with the top 20,000 compounds considered for further analysis. The diversity-based selection method grouped compounds into 300 clusters (Tc < 0.5 maximum similarity between compounds). Compounds with a net charge of more than +2 were discarded, and strain energy scoring combined with visual inspection was used to narrow down a final diverse set of 210 compounds. Of these, 170 compounds were tested in-house, resulting in two hit compounds, Compound **4** and **5**, with IC50 values of 55.7 μM and 57.1 μM, respectively (Figures 6B and 6C). Redocking of both virtual hit compounds showed reasonable overlay with the in-house crystallographic pose (data not shown). Interestingly, molecular docking of Compound **5** to the USP30 structure revealed that the trifluoromethyl ($CF_3$) functional group was predicted to be in the close proximity to the catalytic cysteine (Cys77) (Figure 7A). This observation led to the hypothesis that engineering a covalent warhead in place of $CF_3$ could enable covalent bond formation with Cys77. Our subsequent docking studies supported this hypothesis, predicting the formation of a covalent bond between Cys77 and the nitrile warhead (Figure 7B). Superposition of the docked covalent complex structure with the in-house co-crystal structure showed a good overlay (Figure 7C). These findings suggest that future medicinal chemistry optimization of compound **5** could focus on validating covalent bond formation with catalytic Cys77, which may effectively inhibit USP30's catalytic activity.

## Discussion

The druggability of USP family is an open question[38]. Our effort towards the systematic analysis of USP family showed indicated a highly dynamic and flexible nature of the enzyme catalytic site, making it challenging to design small molecules that can bind effectively and selectively (data not shown). The active sites of many USP enzymes are also shallow or lack well-defined pockets, further complicating the identification of suitable binding sites for drug development. Additionally, the ubiquitin-proteasome system is tightly regulated and involves multiple complex interactions, making it difficult to modulate the function of USPs without disrupting other cellular processes. As a result, targeting USP family members for therapeutic intervention requires overcoming significant structural and functional challenges. USP30, a deubiquitinase enzyme primarily located in the mitochondria, holds significant clinical importance due to its potential therapeutic benefits across various diseases. As such, developing selective USP30 inhibitors could provide new avenues for improving patient outcomes in both neurodegenerative disorders and cancers. Several inhibitors of USP30 have been reported in the literature[21,39] (for review please see[40]), with the most-well characterized being a series of small molecules developed by Vincere Biosciences and cyanopyrrolidines (developed by Mission Therapeutics)[22,23,41]. However, peptidomimetic inhibitors, designed to mimic peptides for therapeutic purposes, present several challenges in drug development. One significant issue is their high molecular weight (> 500 Da), which can hinder effective absorption, distribution, and cellular penetration, metabolic stability, limiting their oral bioavailability[42]. Moreover, the high molecular weight of peptidomimetics can increase the likelihood of immunogenic reactions[43,44] as the body may recognize these molecules as foreign entity, potentially triggering an immune response. Furthermore, cyanopyrrolidines compounds shown to become less specific at higher concentrations which may pose challenges if cellular uptake and target engagement efficiency is unknown[21,22,23]. These factors complicate the development and clinical application of inhibitors, requiring careful optimization to balance efficacy and safety. Despite the challenges posed by the small and relatively imbalanced hydrophilic/hydrophobic nature of the USP30 catalytic pocket, this study highlights the key structural characteristics relevant for inhibitor design. The ability of compound **1** to dock successfully within the catalytic pocket following induced-fit effects highlights the significance of accounting for dynamic structural changes when designing inhibitors. Analysis of published small molecule-bound USP family protein structures reveal a recurring feature: many USP inhibitors utilize a phenyl ring that deeply inserts into the P4 sub-pocket of the catalytic site, a region occupied by

Leu73 in the natural substrate. The substrate sequence, encompassing Leu71-Arg72-Leu73-Arg74-Gly75-Gly76, suggests that binding heavily depends on the two arginine residues forming multiple charge or polar interactions with the enzyme. For USP30, the catalytic site, consisting of Cys77 and His452 where ubiquitin in bound, is characterized by its small size and low hydrophobic/hydrophilic balance, which complicates virtual screening efforts. Compounds from Vincere Bioscience, for example, are relatively large and contain multiple hydrophobic groups, making it difficult for them to fit into the binding pocket without inducing conformational changes. Based on the crystal structure of USP30 in complex with ubiquitin (USP30-Ub), we found that manual modelling followed by induced-fit docking enabled compound **1** to achieve a reasonable fit within the catalytic pocket. Further, acquiring a co-crystal structure of USP30 in complex with a small molecule inhibitor is crucial for advancing our understanding of the protein-ligand interaction at a molecular level. Our in-house structural biology effort resulted in the co-crystal structure of USP30 bound to a covalent inhibitor developed by Mission Therapeutics. The structural data provides detailed insights into the binding mode, key interactions, and conformational changes upon inhibitor binding in relative to that from Ub-bound state, validating our modelling hypothesis and providing a high-resolution structural template for carrying out a 2$^{nd}$ round of virtual screening. From the two rounds of virtual screens, we obtained new chemical scaffolds featuring indole, chloro benzamide and benzothiazole sulfonamide. These inhibitors were predicted to bind within the USP30 catalytic site non-covalently, engaging mainly hydrophobic and polar interactions with the active site residues. Our in-house medicinal chemistry studies showed that a covalent interaction is indispensable for the mission therapeutics compound and when the covalent warhead was removed (data not shown), the inhibitory potency of the inhibitor was abolished. These results highlight the importance for a small molecule inhibitor capable of fully utilizing its pharmacophore to form high affinity binding with surround residues, a challenge that is beyond the scope of this study- hit to lead modification based on current scaffolds. On the other hand, although the molecules reported here are weak inhibitors of USP30, they may still hold promise for further development as a PROTACs (Proteolysis Targeting Chimera) by linking it to a ligand that recruits an E3 ligase such as cereblon. PROTACs are bifunctional molecules designed to harness the cell's ubiquitin-proteasome system to selectively degrade specific proteins. This approach maybe highly recommended for protein targets that are intractable for small molecule inhibition. Thus, even suboptimal inhibitors can be transformed into powerful tools for targeted degradation, expanding their therapeutic potential. In summary, our work provides a framework on molecular modelling for USP30 and potentially the approach may be

translated into other family members of other USPs. We also report the co-crystal structure of small inhibitor bound to USP30. Together with the chemical scaffolds that represent for the first time, non-covalent USP30 inhibitors, lay a crucial foundation for future medicinal chemistry optimization towards the discovery and development of potent and selective USP30 inhibitors to address the unmet need for effective therapeutics targeting mitochondrial dysfunction associated with IPF and related diseases.

**Graphical Abstract**

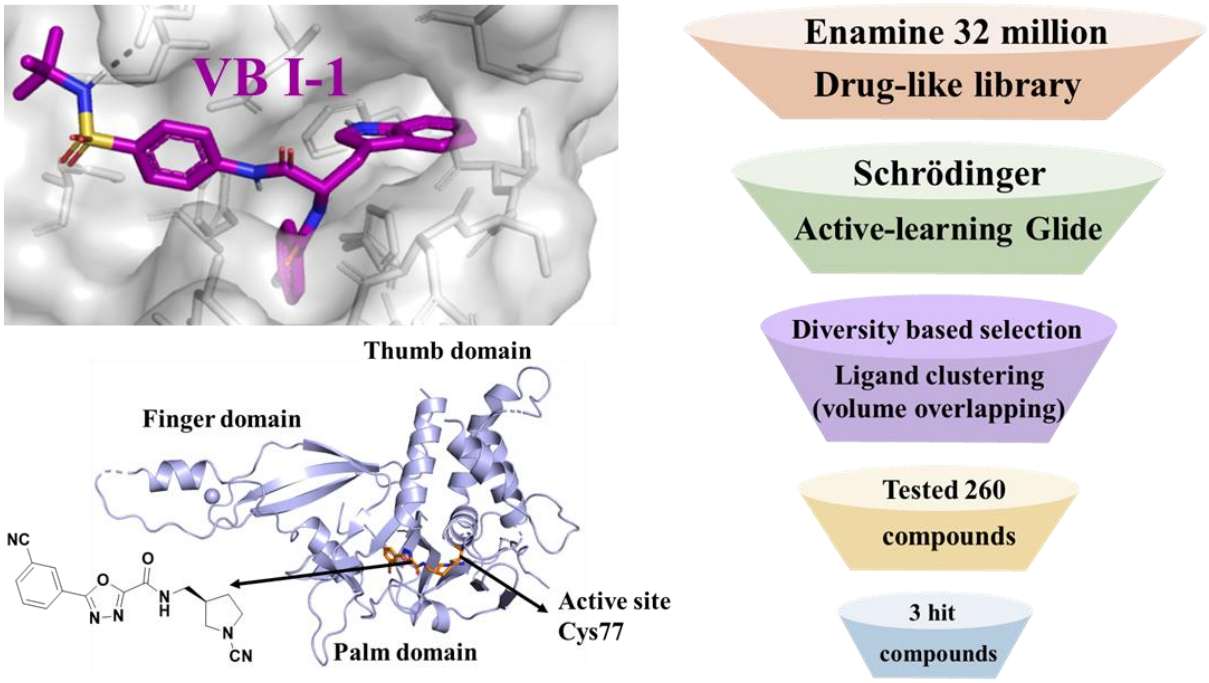

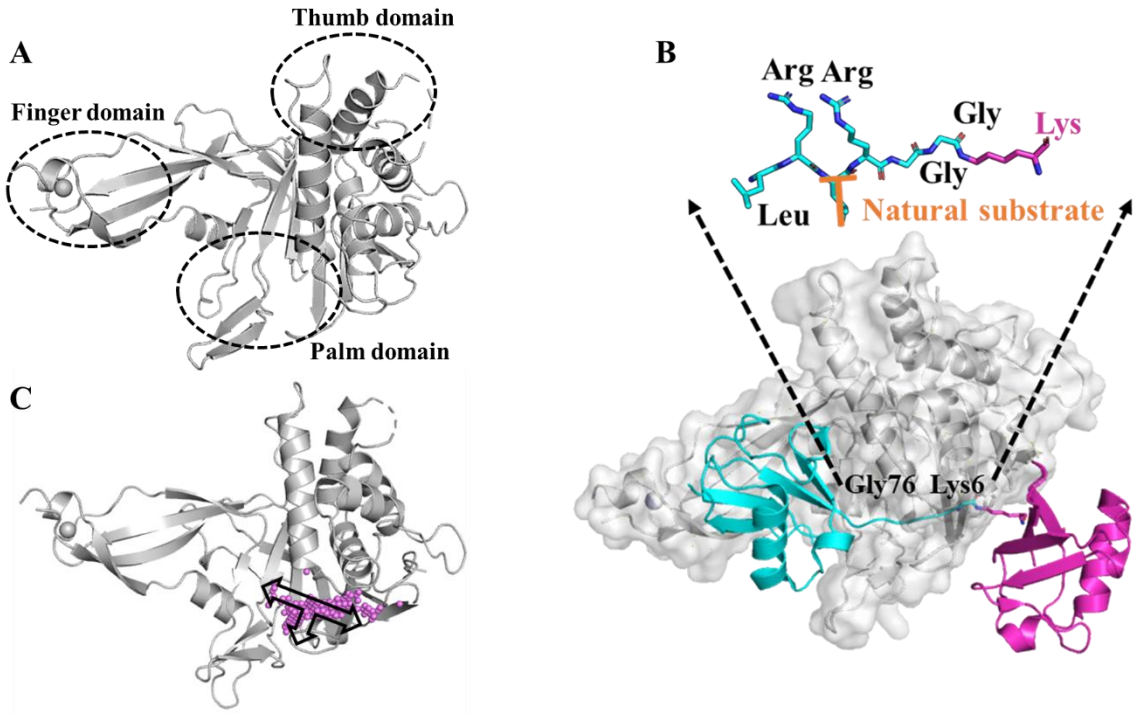


**Figure 1:** A) The crystal structure of human USP30 (PDB ID: 5OHP) showing the thumb, finger and palm domains. B) USP30 in complex with Lys6-diUbiquitin (cyan and magenta), the natural substrate residue Lue73, which adopts a "T" shaped conformation (highlighted in orange) that fits into the deep pocket of the active-site. C) Sitemap analysis of USP30 was performed after the removal of the diubiquitin, yielding a DScore of 0.995. The sitemap identified residues include Asp447, Met448, His449, Ser450, Phe453, Ser493, Tyr495, His324, Gln326, Arg327, Leu328, Glu158, Glu159, Gln160, Asp161, Ala162, Lys338, Arg339, His340 and His444.

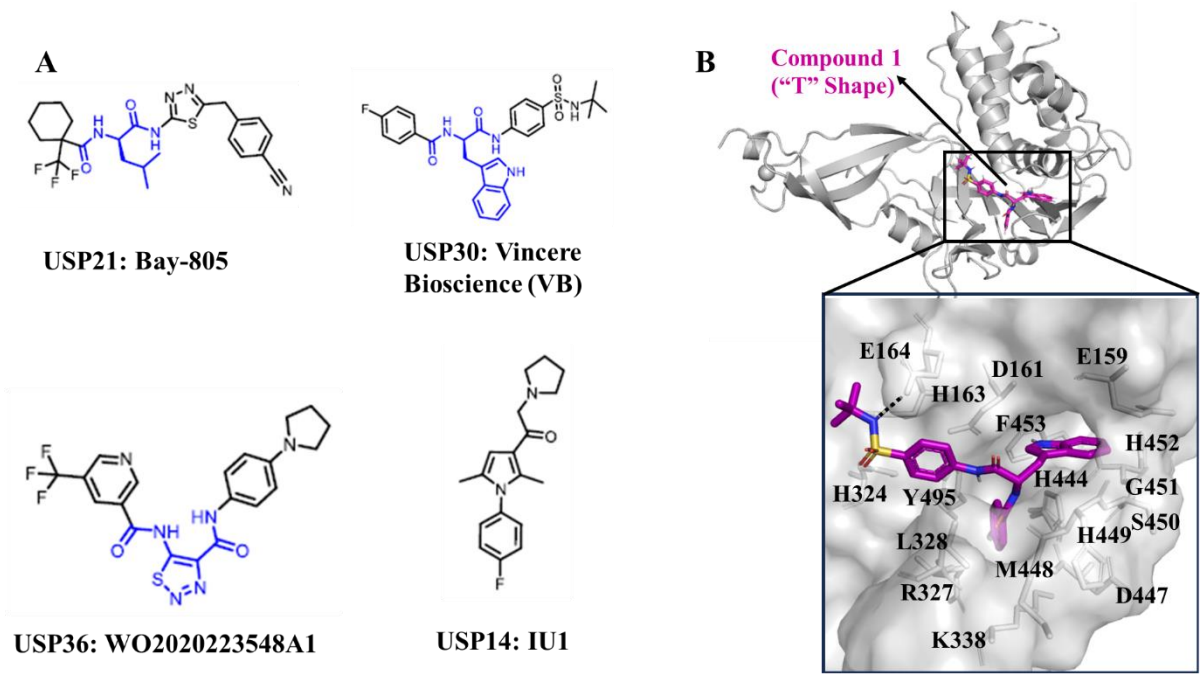


**Figure 2:** A) The list of reported USP inhibitors for USP21, USP30, USP36 and USP14. B) Induced-fit docked pose of the compound **1**. The inset highlights the fluorobenzene group positioned fitting deeply into the pocket, with the sulfonamide moiety positioned to the left and the indole to the right side of the pocket. The NH group of the sulfonamide forming an H-bond interaction with Glu164 is shown. Overall, this binding pose mimics the "T" shaped conformation of the natural substrate.

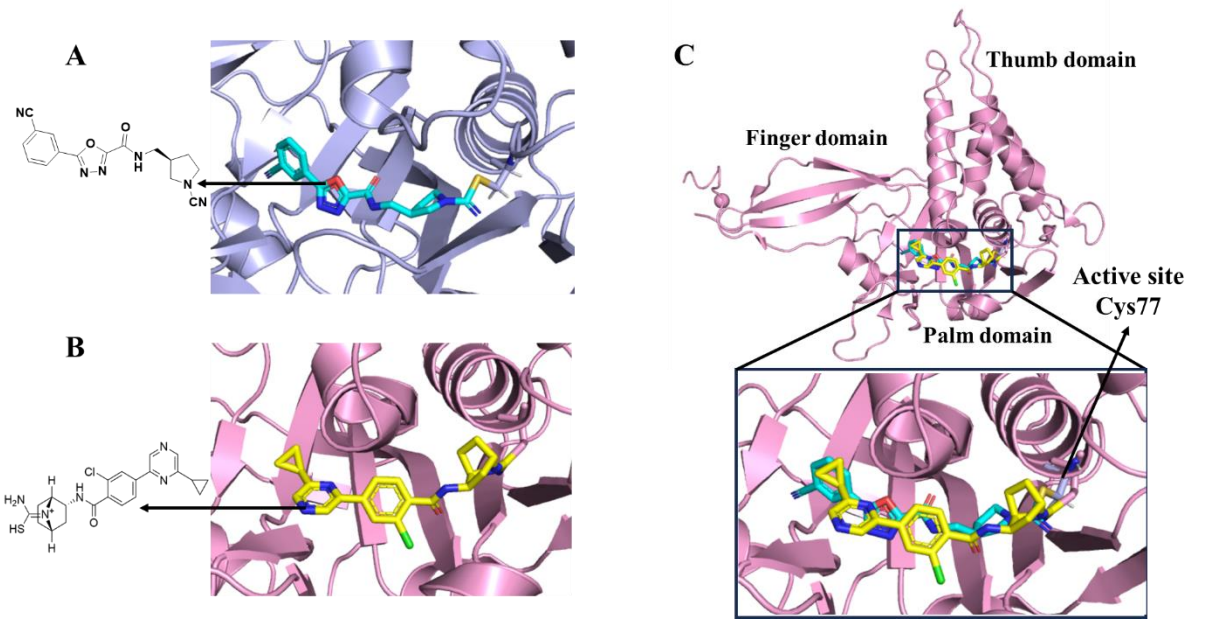


**Figure 3:** A) Compound **2** (Mission Therapeutics) covalently docked to the compound **1** (Vincere Biosciences) trained USP30 structure. B) Overlay of the docked complex with the in-

house solved co-crystal structure, showing the compound bound within the catalytic pocket with a 1.6Å difference between the docked and co-crystal pose. C) Crystal structure of human USP30 in complex with a covalent inhibitor 829 (PDB ID: 8D0A). D) Over lay of the docked compound **2** with the USP30 co-crystal structure of the covalent inhibitor (PDB ID: 8D0A), demonstrating a good alignment of binding modes. Both in-house x-ray structure and the published co-crystal structure validate the docking predictions.

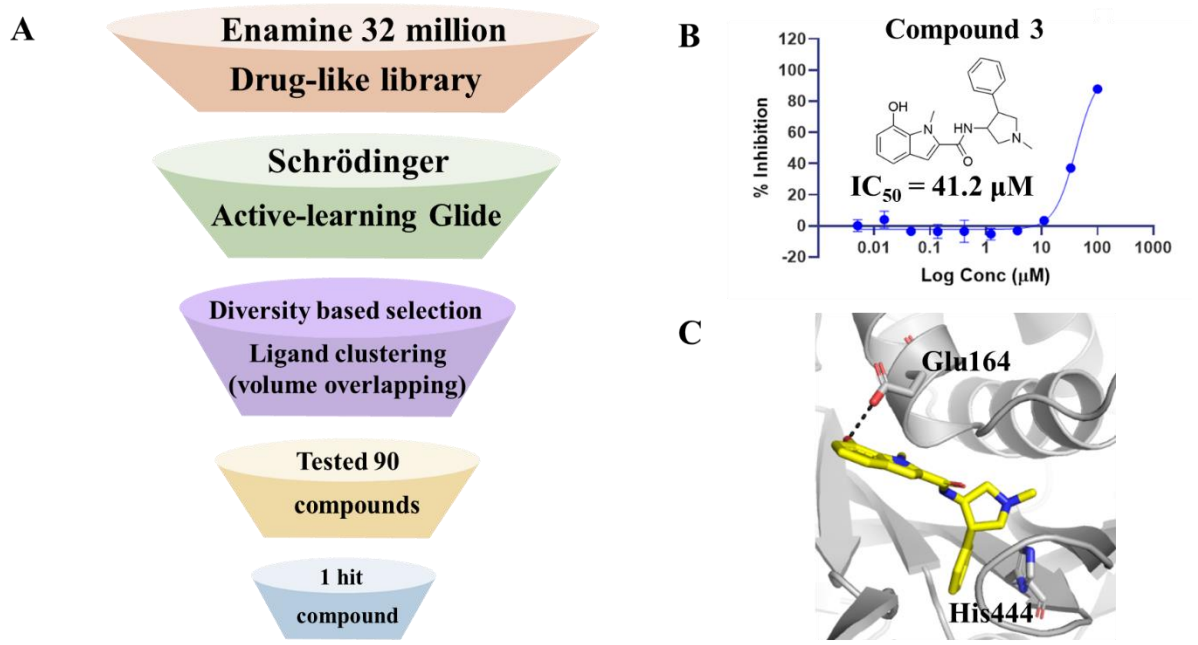


**Figure 4:** A) Workflow of the first round of virtual screening (VS) performed using the compound **1** trained model. Compounds were prioritized based on diversity-based selection, ligand clustering (volume overlapping) and charge constraints (total charge not ≤ 2). A total of 90 compounds were tested in-house. B) One hit compound **3**, exhibited an $IC_{50}$ of 41.2 µM. C) Redocking compound **3** to the USP30 shows the phenyl ring of the compound forming a stacking interaction with His444. An H-bond interaction with Glu164 is indicated by yellow dashed lines.

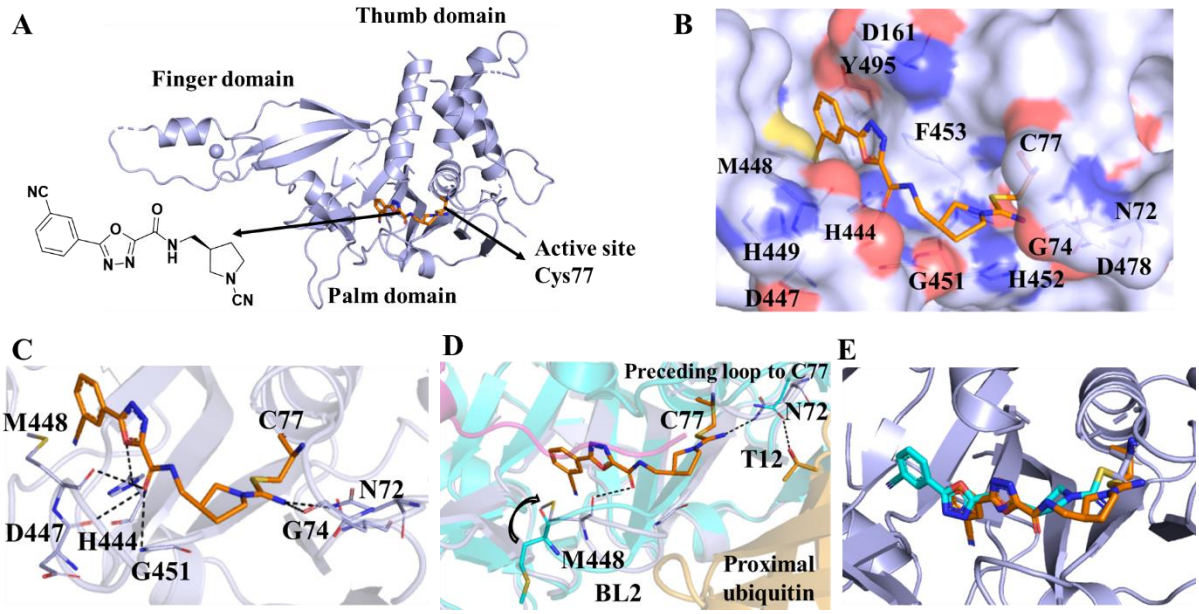


**Figure 5**: A) Crystal structure of the USP30 catalytic domain co-purified with compound **2**, showing covalent modification of Cys77 by compound **2** (orange). B) Surface representation of USP30 binding pocket of compound **2**. Residues lining the binding pocket (<4 Å) are displayed as sticks. C) Hydrogen bond interactions between compound **2** and USP30 are indicated by black dashed lines. D) Superposition of USP30 catalytic domain (CD)-compound **2** complex (light blue) with the USP30-Lys6-diubiquitin complex (PDB ID: 5OHP; USP30 in cyan, distal ubiquitin in magenta and proximal ubiquitin in orange). Compound **2** binds at the thumb-palm cleft, which guides the ubiquitin C-terminus into the active site. Repositioning of the Met448 side chain in the USP30-compound **2** complex is highlighted with a black arrow, and a hydrogen bond between Asn72 of USP30 and compound **2** is shown.

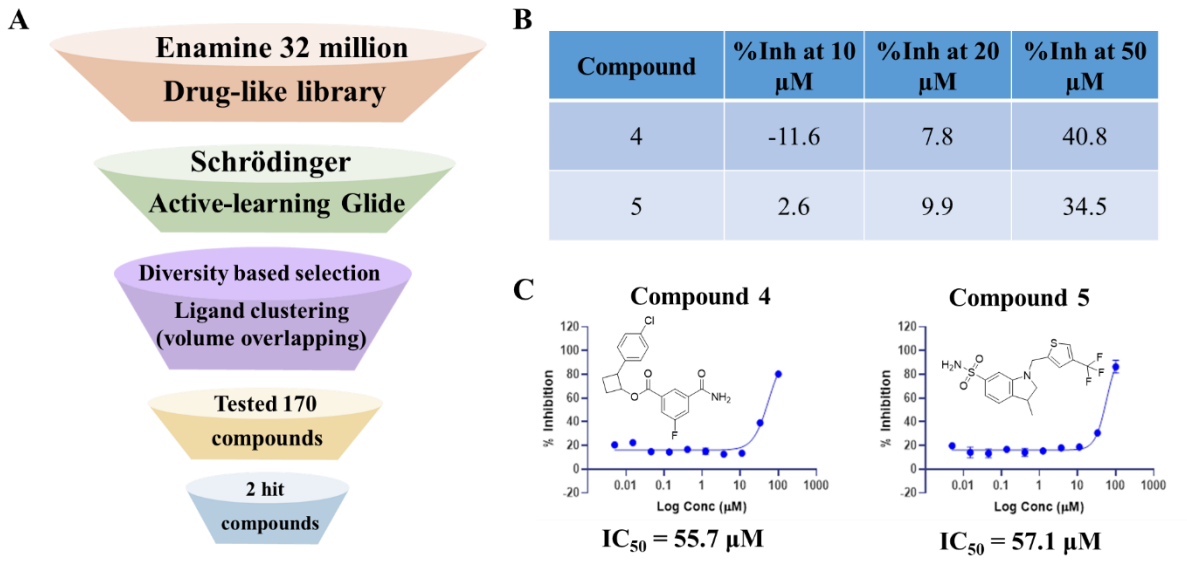


| Compound | %Inh at 10 μM | %Inh at 20 μM | %Inh at 50 μM |
|---|---|---|---|
| 4 | -11.6 | 7.8 | 40.8 |
| 5 | 2.6 | 9.9 | 34.5 |

**Figure 6:** A) Workflow of the second round of virtual screening (VS) performed using the in-house USP30 X-ray structure. Compounds were prioritized based on diversity-based selection, ligand clustering (volume overlapping), and charge constraints (total charge ≤ 2). A total of 120 compounds were tested in-house, resulting in the identification of two weak hits. B) Percent inhibition at 10 μM, 20 μM and 50 μM for the two virtual hits is shown. C) Two compounds, compound **4** and compound **5** exhibited an $IC_{50}$ values of 55.7 μM and 57.1 μM respectively.

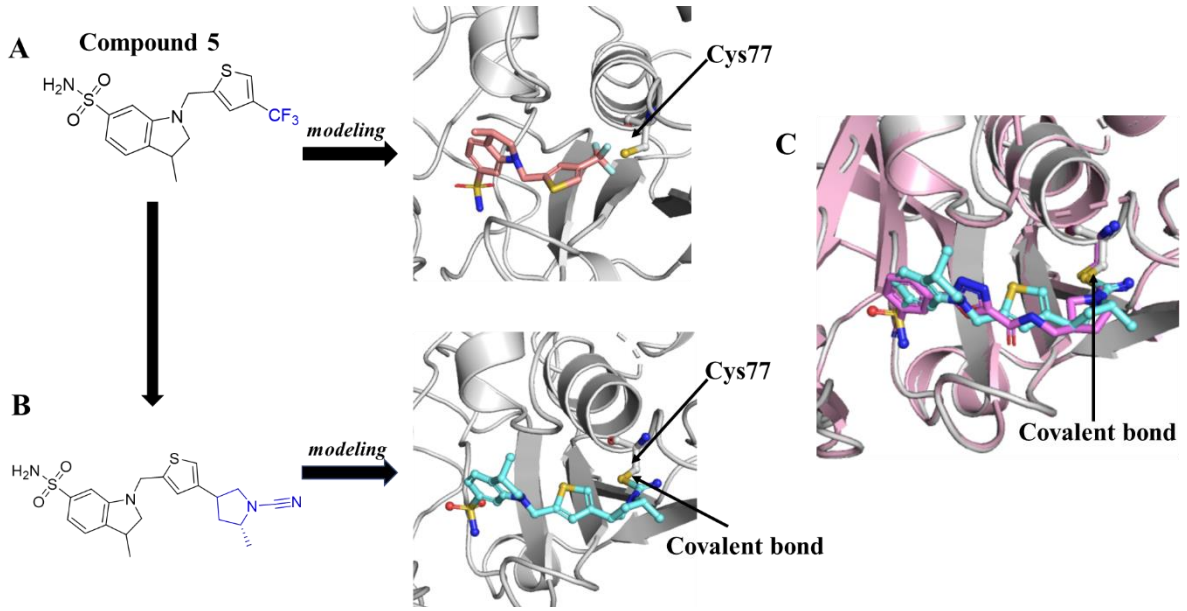


**Figure 7:** A) Docking of the virtual hit (compound **5**) to the in-house x-ray structure predicted that CF3 group is in the close proximity to catalytic Cys77 residue. B) Compound **5** was modified with a nitrile warhead and covalently docked to the in-house USP30 x-ray structure, suggesting potential covalent bond formation with Cys77. C) Overlay of engineered compound

(purple) to the in-house x-ray structure (light pink) shows alignment, indicating the engineered compound may form a covalent interaction with the catalytic Cys77 residue.

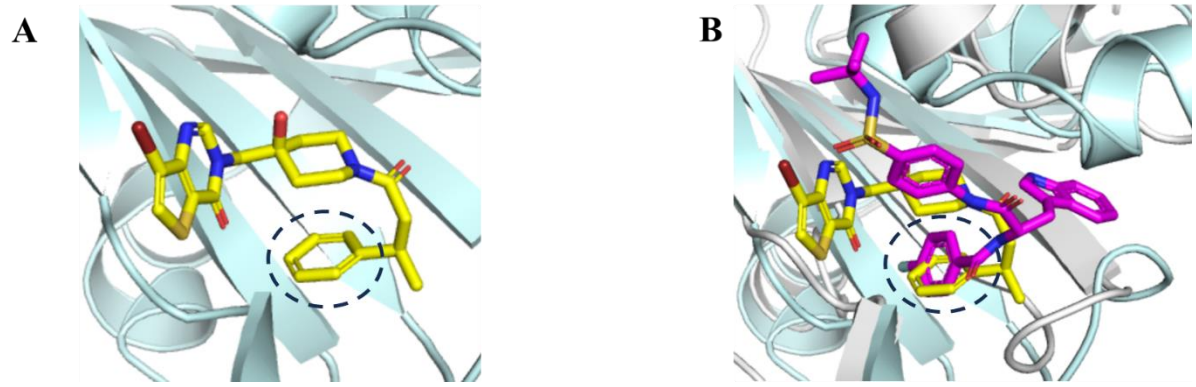


**Supplementary figure 1**: A) Co-crystal structure of USP7 (pale cyan) bound to an inhibitor (yellow; PDB ID: 5N9R) B) Overlay of USP30 docked complex (compound **1** shown in purple) with the USP7 co-crystal structure, highlighting the phenyl ring occupying the deep pocket (indicated by a black dotted circle).

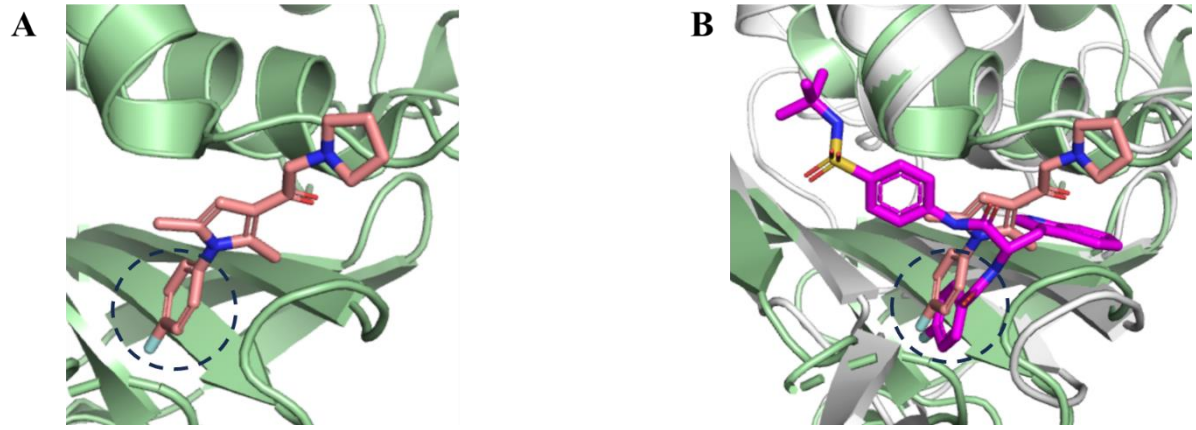


**Supplementary figure 2**: A) Co-crystal structure of USP14 (pale green) bound to an inhibitor (salmon; PDB ID: 6IIK). B) Overlay of USP30 docked complex (compound **1** shown in purple) to the USP14 co-crystal structure, highlighting the phenyl ring occupying the deep pocket (indicated by a black dotted circle).

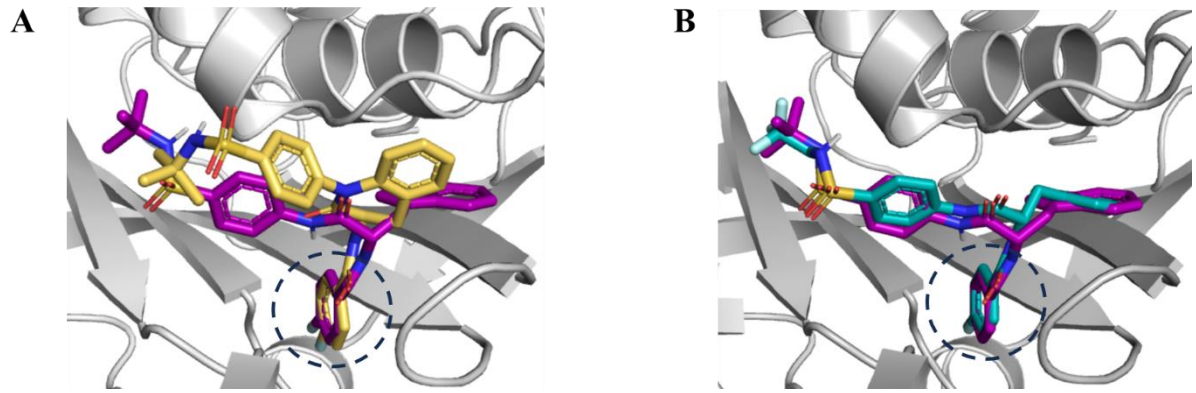


**Supplementary figure 3**: A) Overlay of compound 1 (purple) and I-20 (yellow-orange). B) Overlay of compound **1** (purple) and I-23 (teal). The phenyl ring occupying the deep pocket indicated by a black dotted circle.

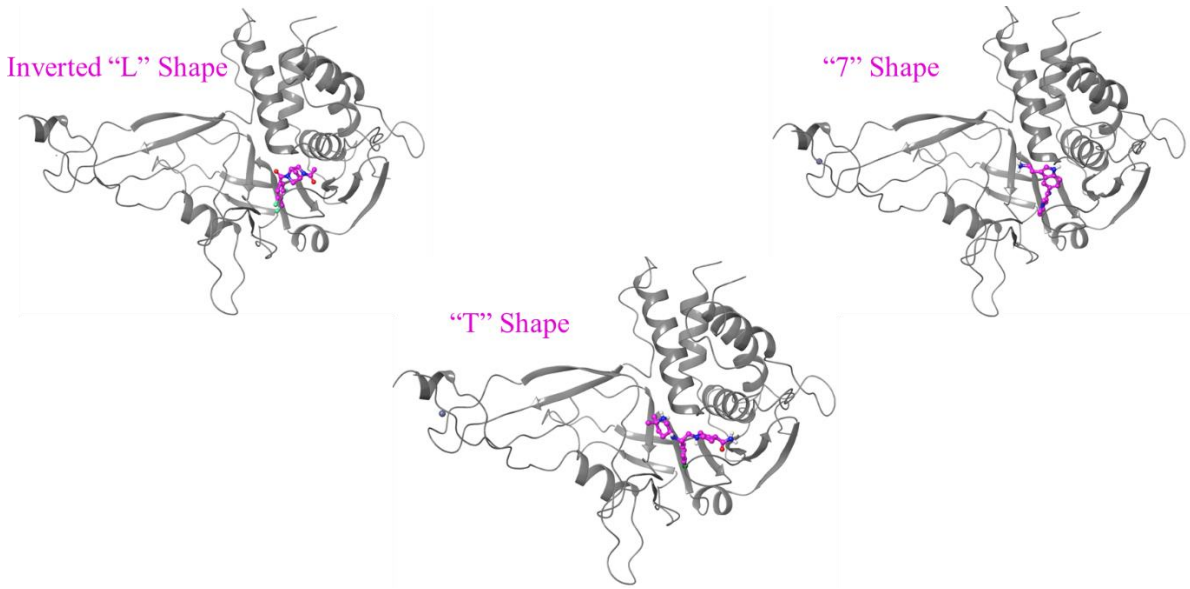


**Supplementary figure 4**: The virtual screening indicates that the compounds predominantly adopted three distinct binding conformations: an inverted "L" shape, a "7" shape and a "T" shape.

**Table 1. Data collection and refinement statistics.**

| USP30-compound **2** complex | |
|---|---|
| Wavelength (Å) | 0.9537 |
| Resolution range (Å) | 39.98 - 2.57 (2.67 - 2.57)* |
| Space group | P 21 21 21 |
| Unit cell | 53.0 60.8 102.5 90 90 90 |
| Total reflections | 21635 (2089) |
| Unique reflections | 10924 (1058) |
| Multiplicity | 2.0 (2.0) |
| Completeness (%) | 99.46 (96.67) |
| Mean I/sigma(I) | 6.43 (0.98) |
| Wilson B-factor | 45.2 |
| R-merge | 0.074 (0.595) |
| R-meas | 0.106 (0.841) |
| R-pim | 0.074 (0.595) |
| CC1/2 | 0.994 (0.471) |
| CC* | 0.998 (0.8) |
| Reflections used in refinement | 10907 (1045) |
| Reflections used for R-free | 1092 (105) |
| R-work | 0.222 (0.317) |
| R-free | 0.276 (0.368) |
| CC(work) | 0.939 (0.685) |
| CC(free) | 0.915 (0.544) |
| Number of non-hydrogen atoms | 2316 |
| Macromolecules | 2299 |
| Ligands | 1 |
| Solvent | 16 |
| Protein residues | 301 |
| RMS(bonds) | 0.005 |
| RMS(angles) | 0.75 |
| Ramachandran favored (%) | 96.13 |
| Ramachandran allowed (%) | 3.87 |
| Ramachandran outliers (%) | 0 |
| Rotamer outliers (%) | 0 |
| Clashscore | 3.64 |
| Average B-factor | 48.31 |
| Macromolecules | 48.39 |
| Ligands | 39.76 |
| Solvent | 36.75 |

*Statistics for the highest-resolution shell are shown in parentheses.

**Acknowledgement:**

*"This research was undertaken in part using the MX2 beamline at the Australian Synchrotron, part of ANSTO, and made use of the Australian Cancer Research Foundation (ACRF) detector"*

## REFERENCES

(1) Harrigan, J. A.; Jacq, X.; Martin, N. M.; Jackson, S. P. Deubiquitylating enzymes and drug discovery: emerging opportunities. Nat Rev Drug Discov 2018, 17 (1), 57-78. DOI: 10.1038/nrd.2017.152

(2) Clague, M. J.; Urbe, S.; Komander, D. Breaking the chains: deubiquitylating enzyme specificity begets function. Nat Rev Mol Cell Biol 2019, 20 (6), 338-352. DOI: 10.1038/s41580-019-0099-1

(3) Nijman, S. M.; Luna-Vargas, M. P.; Velds, A.; Brummelkamp, T. R.; Dirac, A. M.; Sixma, T. K.; Bernards, R. A genomic and functional inventory of deubiquitinating enzymes. Cell 2005, 123 (5), 773-786. DOI: 10.1016/j.cell.2005.11.007

(4) Komander, D.; Clague, M. J.; Urbe, S. Breaking the chains: structure and function of the deubiquitinases. Nat Rev Mol Cell Biol 2009, 10 (8), 550-563. DOI: 10.1038/nrm2731

(5) Hu, M.; Li, P.; Li, M.; Li, W.; Yao, T.; Wu, J. W.; Gu, W.; Cohen, R. E.; Shi, Y. Crystal structure of a UBP-family deubiquitinating enzyme in isolation and in complex with ubiquitin aldehyde. Cell 2002, 111 (7), 1041-1054. DOI: 10.1016/s0092-8674(02)01199-6

(6) Cunningham, C. N.; Baughman, J. M.; Phu, L.; Tea, J. S.; Yu, C.; Coons, M.; Kirkpatrick, D. S.; Bingol, B.; Corn, J. E. USP30 and parkin homeostatically regulate atypical ubiquitin chains on mitochondria. Nat Cell Biol 2015, 17 (2), 160-169. DOI: 10.1038/ncb3097

(7) Ordureau, A.; Sarraf, S. A.; Duda, D. M.; Heo, J. M.; Jedrychowski, M. P.; Sviderskiy, V. O.; Olszewski, J. L.; Koerber, J. T.; Xie, T.; Beausoleil, S. A.; Wells, J. A.; Gygi, S. P.; Schulman, B. A.; Harper, J. W. Quantitative Proteomics Reveal a Feedforward Mechanism for Mitochondrial PARKIN Translocation and Ubiquitin Chain Synthesis. Mol. Cell 2014, *56* (3), 360–375. DOI: 10.1016/J.MOLCEL.2014.09.007

(8) Kubli, D. A.; Gustafsson, Å. B. Mitochondria and Mitophagy: The Yin and Yang of Cell Death Control. *Circ. Res.* 2012, *111* (9), 1208–1221. DOI: 10.1161/circresaha.112.265819

(9) Narendra, D.; Walker, J. E.; Youle, R. Mitochondrial quality control mediated by PINK1 and Parkin: links to parkinsonism. Cold Spring Harb Perspect Biol 2012, 4 (11). DOI: 10.1101/cshperspect.a011338

(10) Fang T. S. Z.; Sun Y.; Pearce A. C.; Eleuteri S.; Kemp M.; Luckhurst C. A.; Williams R.; Mills R.; Almond S.; Burzynski L.; Márkus N. M.; Lelliott C. J.; Karp N. A.; Adams D. J.; Jackson S. P.; Zhao J. F.; Ganley I. G.; Thompson P. W.; Balmus G.; Simon D. K. Knockout or inhibition of USP30 protects dopaminergic neurons in a Parkinson's disease mouse model. Nat Commun 2023, 14(7295). DOI: 10.1038/s41467-023-42876-1

(11) Tsubouchi, K.; Araya, J.; Kuwano, K. PINK1-PARK2-mediated mitophagy in COPD and IPF pathogeneses. Inflamm Regen 2018, 38, 18. DOI: 10.1186/s41232-018-0077-6

(12) Siekacz, K.; Piotrowski, W. J.; Iwański, M. A.; Górski, P.; Białas, A. J. The role of interaction between mitochondria and the extracellular matrix in the development of idiopathic pulmonary fibrosis. Oxid Med Cel Longev 2021, 18, 9932442–9932512. DOI:10.1155/2021/993244

(13) Bingol, B.; Tea, J. S.; Phu, L.; Reichelt, M.; Bakalarski, C. E.; Song, Q.; Foreman, O.; Kirkpatrick, D. S.; Sheng, M. The mitochondrial deubiquitinase USP30 opposes parkin-mediated mitophagy. Nature 2014, 510 (7505), 370-375. DOI: 10.1038/nature13418

(14) Marcassa, E.; Kallinos, A.; Jardine, J.; Rusilowicz-Jones, E. V.; Martinez, A.; Kuehl, S.; Islinger, M.; Clague, M. J.; Urbe, S. Dual role of USP30 in controlling basal pexophagy and mitophagy. EMBO Rep 2018, 19 (7). DOI: 10.15252/embr.201745595

(15) Chen, S.; Liu, Y.; Zhou, H. Advances in the Development Ubiquitin-Specific Peptidase (USP) Inhibitors. Int J Mol Sci 2021, 22 (9). DOI: 10.3390/ijms22094546

(16) https://patents.google.com/patent/WO2022192562A1/en.

(17) https://vincerebio.com/news-data/Vincere-ADPD-2022.pdf

(18) https://vincerebio.com/news.

(19) Mission Therapeutics Nominates First Development Candidates Targeting USP30. https://missiontherapeutics.com/mission-therapeutics-nominates-first-development-candidates-targeting-usp30/. (accessed 17 January 2025).

(20) Mission Therapeutics announces US FDA approval to initiate Phase II clinical trial of its lead asset MTX652 in Acute Kidney Injury–Mission Therapeutics, accessed 17 January 2025, https://missiontherapeutics.com/mission-therapeutics-announces-us-fda-approval-to-initiate-phase-ii-clinical-trial-of-its-lead-asset-mtx652-in-acute-kidney-injury/

(21) Rusilowicz-Jones, E. V.; Barone, F. G.; Lopes, F. M.; Stephen, E.; Mortiboys, H.; Urbé, S.; Clague, M. J. Benchmarking a Highly Selective USP30 Inhibitor for Enhancement of Mitophagy and Pexophagy. *Life Sci. Alliance* 2021, *5* (2), e202101287. DOI: 10.26508/LSA.202101287.

(22) Phu, L.; Rose, C. M.; Tea, J. S.; Wall, C. E.; Verschueren, E.; Cheung, T. K.; Kirkpatrick, D. S.; Bingol, B. Dynamic Regulation of Mitochondrial Import by the Ubiquitin System. Mol. Cell 2020, *77*, 1107–1123.e10. DOI: 10.1016/j.molcel.2020.02.012

(23) Tsefou, E.; Walker, A. S.; Clark, E. H.; Hicks, A. R.; Luft, C.; Takeda, K.; Watanabe, T.; Ramazio, B.; Staddon, J. M.; Briston, T.; et al. Investigation of USP30 Inhibition to Enhance Parkin-Mediated Mitophagy: Tools and Approaches. Biochem. J. 2021, *BCJ20210508*. DOI: 10.1042/bcj20210508

(24) Gersch, M.; Gladkova, C.; Schubert, A. F.; Michel, M. A.; Maslen, S.; Komander, D. Mechanism and regulation of the Lys6-selective deubiquitinase USP30. Nat Struct Mol Biol 2017, *24* (11), 920-930. DOI: 10.1038/nsmb.3475

(25) Schrödinger Release 2022-3: Schrödinger, L., New York, NY, 2022

(26) Halgren, T. A. Identifying and characterizing binding sites and assessing druggability. J Chem Inf Model 2009, *49* (2), 377-389. DOI: 10.1021/ci800324m

(27) McPhillips, T. M.; McPhillips, S. E.; Chiu, H. J.; Cohen, A. E.; Deacon, A. M.; Ellis, P. J.; Garman, E.; Gonzalez, A.; Sauter, N. K.; Phizackerley, R. P.; Soltis, S. M.; Kuhn, P. Blu-Ice and the Distributed Control System: software for data acquisition and instrument control at macromolecular crystallography beamlines. *J. Synchrotron Radiat* 2002, *9* (Pt 6), 401-406. DOI: 10.1107/s0909049502015170

(28) Kabsch, W. Integration, scaling, space-group assignment and post-refinement. *Acta Crystallogr D Biol Crystallogr* 2010, *66* (Pt 2), 133-144. DOI: 10.1107/S0907444909047374

(29) McCoy AJ,; Grosse-Kunstleve RW,; Adams PD,; Winn MD,; Storoni LC,; Read RJ. Phaser crystallographic software. J Appl Crystallogr 2007, *40* (Pt 4), 658-74 DOI: 10.1107/S0021889807021206

(30) Emsley, P.; Lohkamp, B.; Scott, W. G.; Cowtan, K. Features and development of Coot. Acta Crystallogr D Biol Crystallogr 2010, *66* (Pt 4), 486-501. DOI: 10.1107/S0907444910007493

(31) Afonine, P. V.; Grosse-Kunstleve, R. W.; Echols, N.; Headd, J. J.; Moriarty, N. W.; Mustyakimov, M.; Terwilliger, T. C.; Urzhumtsev, A.; Zwart, P. H.; Adams, P. D. Towards automated crystallographic structure refinement with phenix.refine. Acta Crystallogr D Biol Crystallogr 2012, *68* (Pt 4), 352-367. DOI: 10.1107/S0907444912001308

(32) Gavory, G.; O'Dowd, C. R.; Helm, M. D.; Flasz, J.; Arkoudis, E.; Dossang, A.; Hughes, C.; Cassidy, E.; McClelland, K.; Odrzywol, E.; Page, N.; Barker, O.; Miel, H.; Harrison, T. Discovery and Characterization of Highly Potent and Selective Allosteric USP7 Inhibitors. Nat. Chem. Biol. 2018, *14* (2), 118–125. DOI: 10.1038/NCHEMBIO.2528

(33) Wang, Y.; Jiang, Y.; Ding, S.; Li, J.; Song, N.; Ren, Y.; Hong, D.; Wu, C.; Li, B.; Wang, F.; He, W.; Wang, J.; Mei, Z. Small Molecule Inhibitors Reveal Allosteric Regulation of USP14 via Steric Blockade. *Cell Res.* 2018, *28* (12), 1186–1194. DOI: 10.1038/S41422-018-0091-X

(34) Faesen AC,; Luna-Vargas MP,; Geurink PP,; Clerici M,; Merkx R,; Van Dijk WJ,; Hameed DS,; El Oualid F,; Ovaa H,; Sixma TK. The differential modulation of USP activity by internal regulatory domains, interactors and eight ubiquitin chain types. Chem Biol 2011, *18* (12), 1550-61. DOI: 10.1016/j.chembiol.2011.10.017

(35) Mevissen, T. E. T.; Komander, D. Mechanisms of Deubiquitinase Specificity and Regulation. Annu Rev Biochem 2017, *86*, 159-192. DOI: 10.1146/annurev-biochem-061516-044916

(36) O'Brien, D. P.; Jones, H. B. L.; Guenther, F.; Murphy, E. J.; England, K. S.; Vendrell, I.; Anderson, M.; Brennan, P. E.; Davis, J. B.; Pinto-Fernández, A.; Turnbull, A. P.; Kessler, B. M. Structural Premise of Selective Deubiquitinase USP30 Inhibition by Small-Molecule Benzosulfonamides. Mol. Cell. Proteomics 2023, *22* (8), 100609. DOI: 10.1016/J.MCPRO.2023.100609

(37) O'Brien, D. P.; Jones, H. B. L.; Shi, Y.; Guenther, F.; Vendrell, I.; Viner, R.; Brennan, P. E.; Mead, E.; Zarganes-Tzitzikas, T.; Davis, J. B.; Pinto-Fernández, A.; England, K. S.; Murphy, E. J.; Turnbull, A. P.; Kessler, B. M. Structural Dynamics of the Ubiquitin Specific Protease USP30 in Complex with a Cyanopyrrolidine-Containing Covalent Inhibitor. bioRxiv 2024, *07.20.604388*; DOI: 10.1101/2024.07.20.604388

(38) Schauer, N. J.; Magin, R. S.; Liu, X.; Doherty, L. M.; Buhrlage, S. J. Advances in Discovering Deubiquitinating Enzyme (DUB) Inhibitors. J. Med. Chem. 2020, *63* (6), 2731–2750. DOI: 10.1021/ACS.JMEDCHEM.9B01138

(39) Kluge, A. F.; Lagu, B. R.; Maiti, P.; Jaleel, M.; Webb, M.; Malhotra, J.; Mallat, A.; Srinivas, P. A.; Thompson, J. E. Novel Highly Selective Inhibitors of Ubiquitin Specific Protease 30 (USP30) Accelerate Mitophagy. Bioorg. Med. Chem. Lett. 2018, *28*, 2655–2659. DOI: 10.1016/J.BMCL.2018.05.013

(40) Wang, F.; Gao, Y.; Zhou, L.; Chen, J.; Xie, Z.; Ye, Z.; Wang, Y. USP30: Structure, Emerging Physiological Role, and Target Inhibition. Front Pharmacol 2022, *13*, 851654. DOI: 10.3389/fphar.2022.851654

(41) Rusilowicz-Jones, E. V.; Jardine, J.; Kallinos, A.; Pinto-Fernandez, A.; Guenther, F.; Giurrandino, M.; Barone, F. G.; McCarron, K.; Burke, C. J.; Murad, A.; et al. USP30 Sets a Trigger Threshold for PINK1-PARKIN Amplification of Mitochondrial Ubiquitylation. Life Sci. Alliance 2020, *3*, e202000768. DOI: 10.26508/lsa.202000768

(42) Nielsen, D. S.; Shepherd, N. E.; Xu, W.; Lucke, A. J.; Stoermer, M. J.; Fairlie, D. P. Orally Absorbed Cyclic Peptides. Chem. Rev. 2017, *117* (12), 8094–8128. DOI: 10.1021/acs.chemrev.6b00838

(43) Lamers, C. Overcoming the Shortcomings of Peptide-Based Therapeutics. Future Drug Discovery 2022, *4* (2). DOI: 10.4155/fdd-2022-0005

(44) Real-Fernandez, F.; Errante, F.; Di Santo, A.; Papini, A. M.; Rovero, P. Therapeutic Proteins Immunogenicity: A Peptide Point of View. Explor. Drug Sci. 2023, *1*, 377–387. DOI: 10.37349/eds.2023.00025